A Wideband Differentially Driven Dual-Polarized Antenna by Using Integrated Six-Port Power Divider

Le-Hu Wen, Steven Gao, *Fellow, IEEE,* Qi Luo, *Member, IEEE,* Wei Hu, *Member, IEEE,* Qingling Yang, *Student Member, IEEE,* Yingzeng Yin, *Member, IEEE,* Xiaofei Ren, and Jian Wu

***Abstract*—A new method to design wideband differentially driven dual-polarized antenna with high common mode suppression and high port isolation is presented. The presented antenna can be equivalent as a combination of a six-port power divider and four crossed folded dipoles. The six-port power divider is composed of two orthogonal input ports and four equal magnitude output ports. Detailed analysis illustrates that the six-port power divider can have wide bandwidth and high isolation under odd mode excitation and high common mode suppression under even mode excitation. Therefore, based on the wideband and high even mode suppressed six-port power divider, a wideband differentially driven dual-polarized antenna is developed with high common mode suppression. To validate the design concept, the proposed antenna was designed, fabricated, and measured. The measured results prove that the antenna has a wide impedance bandwidth of 1.64-3.0 GHz (58.6%) for the return loss higher than 15 dB and isolation higher than 35.4 dB. In addition, very high common mode suppression is achieved for the measured common mode reflection coefficient higher than -0.87 dB over the entire bandwidth. With stable antenna gain and half power beamwidth, the develop antenna is suitable for base station applications.**

***Index Terms*—Differentially driven, dual-polarized antenna, even mode, odd mode, power divider.**

I. Introduction

DUAL-POLARIZED antennas have attracted many attentions owing to their advantages of low multi-fading effect and high channel capacity to the wireless communication systems, such as base stations, satellites, and radars systems [1]-[2]. As the development of these communication systems, more and more strict specifications are put forward to meet these different systems requirements, including the compact antenna size, wide impedance bandwidth, high isolation, stable radiation patterns, etc.

Patch antennas are the commonly used techniques to realize dual-polarization with low profile and compact size [3]-[14]. To obtain wide impedance bandwidth, direct probe feed [3]-[4], proximity coupling [5]-[7], aperture coupling [8]-[12], and hybrid feed [13]-[14] are utilized to design wideband dual-polarized antennas. In [4], two stacked E-shaped patches are directly fed by the two probes with the relative bandwidth of 7.7%. By using broadband baluns and proximity coupling, relative bandwidth of 29% is achieved for the antenna in [8]. In addition, crossed slots and copper pillars [10] are used to enhance the isolation of the dual-polarization. However, the bandwidth of patch antennas is normally limited due to the low profile configuration and innate high Q resonance of the patches.

To meet the wider bandwidth requirement, such as the base station applications, dipole antennas [15]-[20] are much preferable compared to the narrow band patch antennas. In [15] and [16], crossed bowtie-shaped dipoles and shared-dipole dual-polarized antennas are presented with wide impedance bandwidth and high isolation. To further increase the impedance bandwidth, stacked parasitic patches [17] and crossed baluns [18]-[19] are integrated into the antennas. In addition, to enhance the cross-polarization of the antenna, parasitic elements are introduced around the dipoles with very low cross-polarization level [20]. However, these are the traditional single-ended dual-polarized antennas. With the development of the differential microwave circuit system, differentially driven antennas are needed to directly connect to these circuit systems. Otherwise, additional baluns or out-of-phase power dividers will be inserted between the differential circuit systems and the traditional single-ended antennas, and this will cause the undesired insertion loss and mismatching between the two different interfaces. Therefore, wideband differentially driven dual-polarized antennas are developed recently [21]-[25]. Owing to the symmetrical differentially driven method, these antennas can have high port isolation. By using parasitic patch and slot excitation, the differentially driven antenna in [21] achieves wide differential impedance bandwidth. With much higher profile of the crown-shaped multi-dipole configuration, the differentially driven antenna [23] obtains the stable beamwidth for base station applications. However, little of these differentially driven antennas are considered about the common mode suppression for these antennas. As one of the important parameters for the differential devices, poor common mode suppression will lead the undesired noises to the circuit system and cause the circuit system a poor signal-to-noise ratio [26].

In this paper, a novel design method of a wideband

This work was supported in part by China Research Institute of Radiowave Propagation, in part by EPSRC grants EP/N032497/1, EP/P015840/1, and EP/S005625/1, and in part by China Scholarship Council. *(Corresponding author: Le-Hu Wen.)*

L.-H. Wen, S. Gao, Q. Luo, and Q. Yang are with the School of Engineering and Digital Arts, University of Kent, Canterbury, CT2 7NT, U.K. (e-mail: lw347@kent.ac.uk)

W. Hu and Y. Yin are with the National Key Laboratory of Antennas and Microwave Technology, Xidian University, Xian, 710071, China.

X. Ren and J. Wu are with the Innovation and Research Center, China Research Institute of Radiowave Propagation, Qingdao, 266107, China.

differentially driven dual-polarized antenna with high common mode suppression is presented. The presented high common mode suppressed antenna is realized by using an integrated wideband high common mode suppressed power divider. The integrated power divider can be equivalent as a six-port network with two orthogonal input ports and four equal magnitude output ports. Detailed working principles of the six-port power divider, including the wideband characteristic and the even-odd mode analysis, are illustrated. Based on the design method, the presented antenna was designed, fabricated, and measured for verification. The measured results show that the impedance bandwidth of the two differentially driven ports is 1.64-3.0 GHz (58.6%) for S_{dd11} and S_{dd22} <-15 dB. Moreover, very high common mode suppression is achieved at the two differentially driven ports with the measured S_{cc11} and S_{cc22} higher than -0.87 dB over the impedance bandwidth.

II. Dual-Polarized Antenna

A. Configuration

The detailed configuration of the presented differentially driven dual-polarized antenna is shown in Fig. 1. The antenna is composed of a square copper sheet as the reflector and a square substrate with both the top and bottom layers printed with the antenna radiator. The antenna is fed by four equal length coaxial cables, which work as the differential feed ports. In Fig. 1 (a), the differential port pair of port 1 and port 2 is designated as the differential port d1 for -45º polarization. While the differential port pair of port 3 and port 4 is designated as the differential port d2 for +45º polarization. To facilitate the analysis of the differentially driven dual-polarized antenna, the differentially and commonly driven S-parameters of the antenna can be expressed as

$$S_{dd11} = (S_{11} + S_{22} - S_{12} - S_{21})/2 \quad (1)$$

$$S_{dd22} = (S_{33} + S_{44} - S_{34} - S_{43})/2 \quad (2)$$

$$S_{dd21} = (S_{31} + S_{42} - S_{32} - S_{41})/2 \quad (3)$$

$$S_{cc11} = (S_{11} + S_{22} + S_{12} + S_{21})/2 \quad (4)$$

$$S_{cc22} = (S_{33} + S_{44} + S_{34} + S_{43})/2 \quad (5)$$

where S_{ij} $(i = 1, 2, 3, 4;\ j = 1, 2, 3, 4)$ are the single-ended S-parameters, which can be obtained from the simulated or measured results. By using (1)-(5), the differentially and commonly driven S-parameters can be directly obtained by using the simulated or measured single-ended S-parameters.

The antenna radiator is printed on a substrate of Rogers 4003C, with the relative dielectric permittivity of 3.55 and the thickness of 0.813 mm. As shown in Fig. 1 (b), the top layer of the substrate is depicted in red color, and the bottom layer is depicted in green color. The main radiating structures of the antenna are four symmetrically arranged folded dipoles. Four via holes are used to connect the top and bottom dipole arms and form four folded dipoles. The four folded dipoles at the periphery are connected to a symmetrical six-port power divider. The detailed configuration of the six-port power divider is shown in Fig. 1 (c). The power divider has two differential input ports for two orthogonal polarizations, and four output ports connected to the peripheral four folded dipoles. Detailed working principles of the six-port power divider will be illustrated in the following sections. The connection method of the feeding coaxial cables to the power divider are also shown in Fig. 1 (c). The outer conductors of the

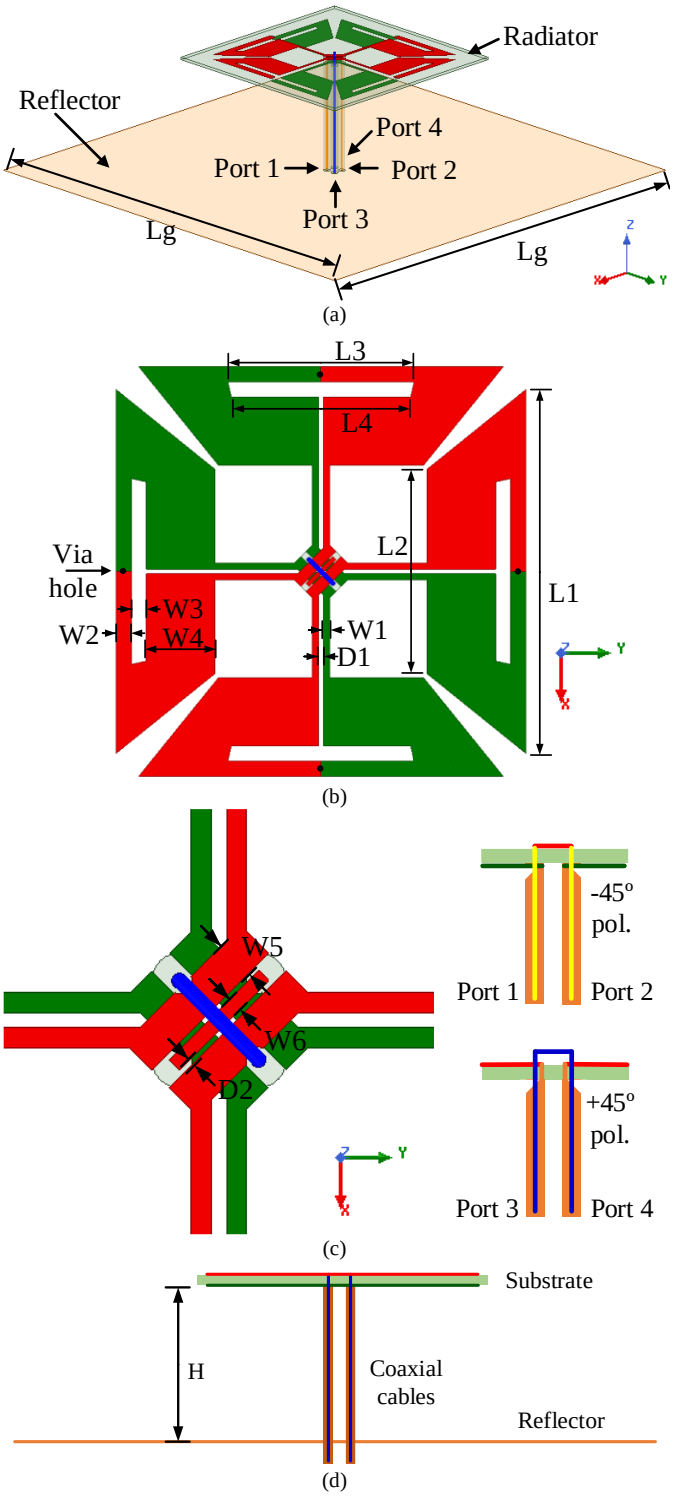

Fig. 1. Configuration of the proposed differentially fed dual-polarized antenna. (a) 3D view. (b). Detailed view of the antenna radiator. (c). Detailed view of the inner six-port power divider. (d). Side view of the antenna. (Detailed parameters of the antenna. Lg=140 mm, L1=48 mm, L2=27 mm, L3=24.5 mm, L4=23.5 mm, W1=0.8 mm, W2=2 mm, W3=2 mm, W4=9 mm, W5=1.5 mm, W6=0.6 mm, D1=0.6 mm, D2=0.2 mm.)

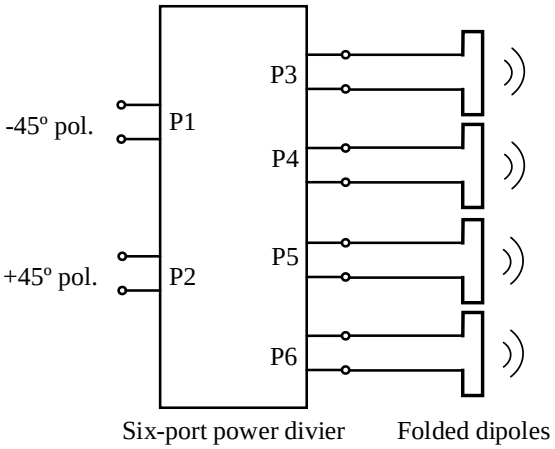

Fig. 2. Equivalent circuit of the proposed antenna.

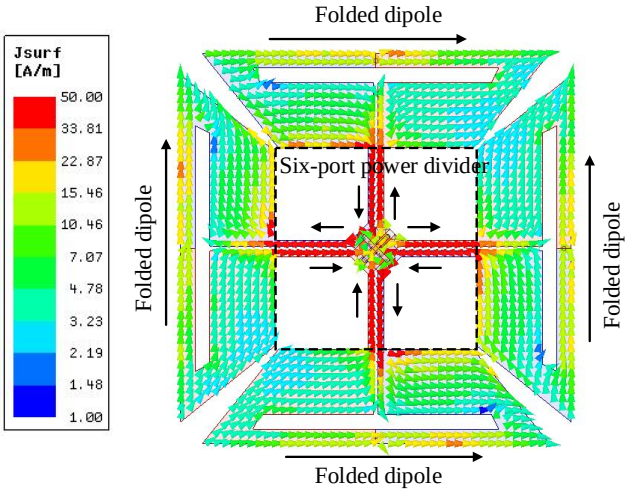

Fig. 3. Current distribution of the proposed antenna at 2.2 GHz when the differential port d1 is excited.

cables are soldered to the two inner arms of the power divider, whereas the inner conductors are connected to each other by themselves or by the top layer strip to avoid feed intersection.

Fig. 1 (d) shows the side view of the antenna. The distance from the top radiator to the bottom reflector is 35 mm, and the size of the square reflector is 140 mm×140 mm. Note that the presented antenna is designed for ±45º polarizations. As a general definition for the ±45º polarized radiation patterns, the xz plane in this paper is defined as the horizontal plane (H-plane), and the yz plane is defined as the vertical plane (V-plane). All the simulation results in this work are obtained by using the electromagnetic simulation software ANSYS HFSS. The detailed parameters of the presented antenna are shown in the caption of Fig. 1.

B. Equivalent Circuit

The presented dual-polarized antenna can be equivalent as a combination of a six-port divider and four folded dipoles for dual-polarization. The equivalent circuit of the proposed antenna is shown in Fig. 2. In the figure, port P1 can be regarded as the differential port d1, which is realized for the -45º polarization. Port P2 can be regarded as the differential port d2, which is realized for the +45º polarization. Whereas the

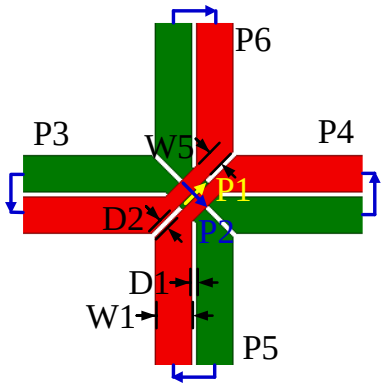

Fig. 4. Simulation model of the six-port power divider. (Detailed parameters of the simulation model. W1=4 mm, D1=-0.8 mm. D2=0.6 mm, W5=1.7 mm.)

ports of P3, P4, P5, and P6 are utilized to drive the four folded dipoles for the operation of the two orthogonal polarizations.

Fig. 3 shows the current distribution of the proposed antenna at 2.2 GHz when differential port d1 is excited for -45º polarization. Auxiliary arrows are added to illustrate the current direction on the antenna surface. Compared to the current magnitude on the four folded dipoles, strong current intensity can be found on the center of the crossed narrow transmission lines. The input power is transmitted to the four folded dipoles by the transmission lines. The four crossed narrow transmission lines in the center work as a six-port power divider with two orthogonal input ports and four equal magnitude output ports. It should be noted that the transmission lines look similar as the traditional parallel transmission lines. However, different from the traditional parallel transmission line, the symmetrical lines (or the center lines) of the two parallel lines are not coincided, and the distance between the two inner edges of the parallel lines is 0.6 mm for the presented antenna. To facilitate the analysis of antenna, this type of the parallel transmission line is designated as the offset parallel transmission line in this work. Detailed working principles about the center six-port power divider, including the wideband characteristic and the even-odd mode analysis, will be illustrated in the following sections.

C. Wideband Six-Port Power Divider

To illustrate the working principle of the six-port power divider, the power divider is extracted out of the presented antenna, and modelled in Fig. 4. In the center of the figure, two lumped ports (P1 and P2) are located at the center with the reference impedance of 50 ohm, which are used to excite the power divider as the input ports. Four wave ports (P3, P4, P5, and P6) at the end of the offset parallel transmission lines are defined as the output ports. Note that the two ends of the port P1 are connected to the bottom strips in green colour, and the two ends of port P2 are connected to the top strips in red colour. Four wave ports are connected at the end of strips with the reference driven direction from the bottom center strips to the top center strips.

Fig. 5 shows the simulated S-parameters of the six-port power divider based on the model shown in Fig. 4. With the parameters provided in the caption of Fig. 4, the characteristic impedance of the offset parallel line is equal to 50 ohm. Owing to the symmetry of the power divider, the magnitudes of the S_{11} and S_{22} are almost same, the magnitudes of the S_{33}, S_{44}, S_{55}, and

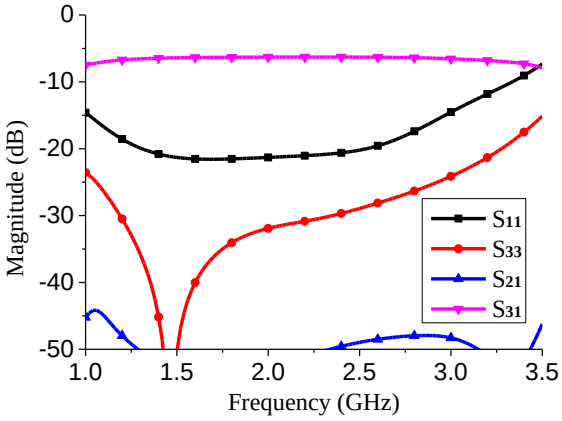

(a)

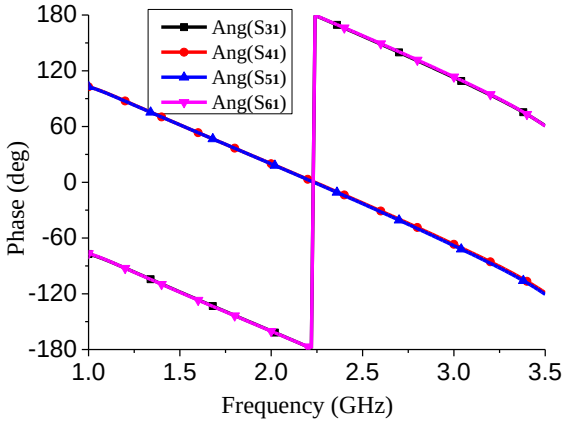

(b)

Fig. 5. Simulated S-parameters of the extracted six-port splitter. (a) Magnitude. (b) Phase.

S_{66} are almost same, and the magnitudes of the S_{31}, S_{41}, S_{51}, S_{61}, S_{32}, S_{42}, S_{52}, S_{62} are also almost same. Therefore, only the magnitudes of S_{11}, S_{33}, S_{21}, S_{31} are given in the figure for clarity.

It can be seen that a wide impedance bandwidth is realized for all the six ports. The simulated overlapped relative bandwidth for all the six ports of the power divider is 100% for the reflection coefficients lower than -15 dB, which covers from 1 GHz to 3 GHz. Stable transmission is obtained from the input port to the four output ports, which is close to the ideal -6 dB. Very high isolation is achieved between the two orthogonal input ports of P1 and P2, which can be utilized to excite the dual-polarized antenna with high isolation. In Fig. 5 (b), out-of-phase is observed for the opposite ports, such as phase (S_{31}) and phase (S_{41}). In addition, in-phase is observed for the adjacent ports, such as phase (S_{31}) and phase (S_{51}). Based on these magnitude and phase characteristics, the six-port power divider can be used to excite the four folded dipoles for the two orthogonal polarizations.

According to the simulated magnitude and phase characteristics, the scattering matrix for this six-port power divider can be concluded as

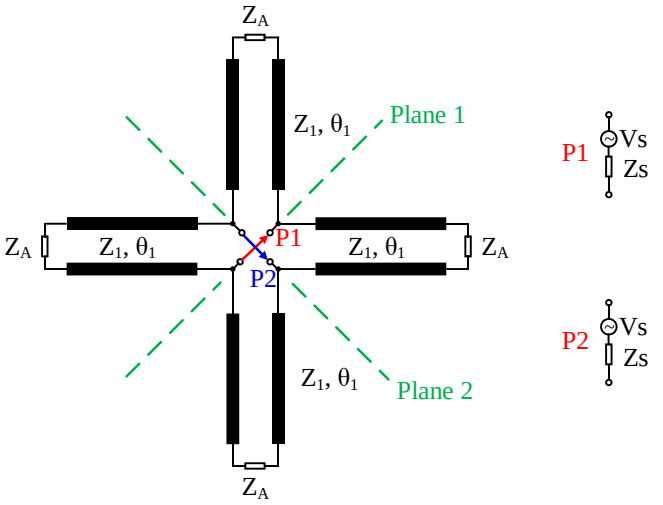

Fig. 6. Transmission line equivalent circuit of the six-port power divider.

$$[S] = \begin{bmatrix} 0 & 0 & -0.5 & 0.5 & 0.5 & -0.5 \\ 0 & 0 & -0.5 & 0.5 & -0.5 & 0.5 \\ -0.5 & -0.5 & 0 & 0 & 0.5 & 0.5 \\ 0.5 & 0.5 & 0 & 0 & 0.5 & 0.5 \\ 0.5 & -0.5 & 0.5 & 0.5 & 0 & 0 \\ -0.5 & 0.5 & 0.5 & 0.5 & 0 & 0 \end{bmatrix} \quad (6)$$

Observing from the matrix, it is can be found that all the input and output ports are well matched. Good isolation can be obtained between the two orthogonal input ports. Four output ports have the same output power with the in-phase or out-of-phase characteristics. A dual-polarized antenna can be realized by using these input and output characteristics. It can be calculated that the scattering matrix also meets the following conditions

$$[S] = [S]^t \quad (7)$$

$$[S]^t[S]^* = [U] \quad (8)$$

where $[S]^t$ is the symmetric matrix of $[S]$, $[S]^*$ is the conjugate matrix of $[S]$, and $[U]$ is the unitary matrix. Therefore, matrix $[S]$ is a symmetric and unitary matrix, and the six-port power divider is a reciprocal and lossless feed network.

D. Even-Odd Mode Analysis

The six-port power divider can be further analyzed by using the equivalent transmission line circuit to get the even-odd mode characteristics. As shown in Fig. 6, the input impedance of the folded dipoles are Z_A, the voltage and impedance of the driven sources of P1 and P2 are Vs and Zs, the characteristic impedance and electric length of the offset parallel lines are Z_1 and θ_1. Two symmetrical planes, Plane 1 and Plane 2, can be found for the presented six-port power divider. Because of the symmetry of the power divider, important impedance characteristics, including the common mode suppression and impedance matching, can be analyzed by using the even-odd mode analysis.

Fig. 7 shows the transmission line equivalent circuit when P1 is driven by the even mode signal. As shown in Fig. 7 (a), because of the even mode excitation at P1, Plane 1 and Plane 2 are equivalent to the open-circuited planes. The load at P2 will

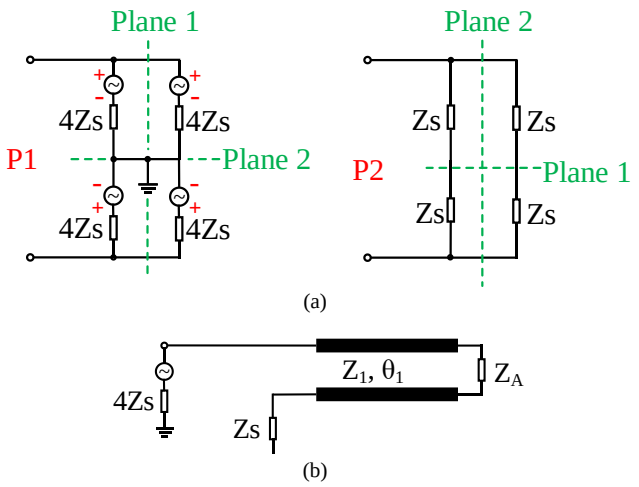

Fig. 7. Even mode analysis of the transmission line equivalent circuit for the six-port power divider when port 1 is excited. (a) Symmetric forms of port 1 and port 2. (b) Simplified even mode excited equivalent circuit.

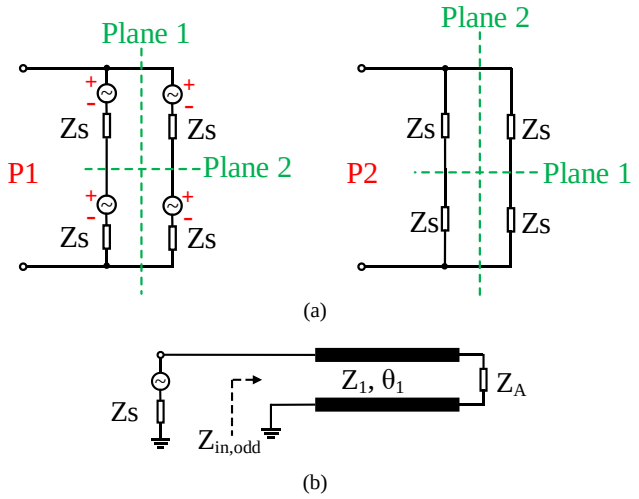

Fig. 8. Odd mode analysis of the transmission line equivalent circuit for the six-port power divider when port 1 is excited. (a) Symmetric forms of port 1 and port 2. (b) Simplified odd mode excited equivalent circuit.

be open-circuited with regard to both two symmetrical planes. Therefore, as shown in Fig. 7 (b), the simplified even mode excited equivalent circuit is driven with a source impedance of $4Z_s$ at P1. The current flowing through this circuit cannot form a loop because of the equivalent open-circuit at P2. This means that it will be totally mismatched for the even mode signal. Therefore, high common mode suppression can be obtained owing to the even mode driven symmetrical six-port power divider, and the reflection coefficient under even mode excitation can be expressed as

$$\Gamma_{1,even} = \infty \tag{9}$$

Fig. 8 shows the transmission line equivalent circuit when P1 is driven by the odd mode signal. As shown in Fig. 8 (a), because of the odd mode excitation at P1, Plane 1 is equivalent as the open-circuited plane, and Plane 2 is equivalent as the short-circuited plane. The load at P2 will be directly shorted to the ground because of the equivalent short-circuit with regard to Plane 2. Therefore, as shown in Fig. 8 (b), the simplified equivalent circuit under odd mode excitation is driven with a

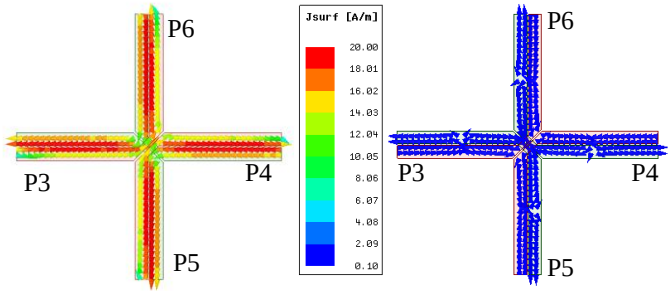

Fig. 9. Current distributions on surface of the six-port power divider. (a) Odd mode excitation at port 1. (b) Even mode excitation at port 1.

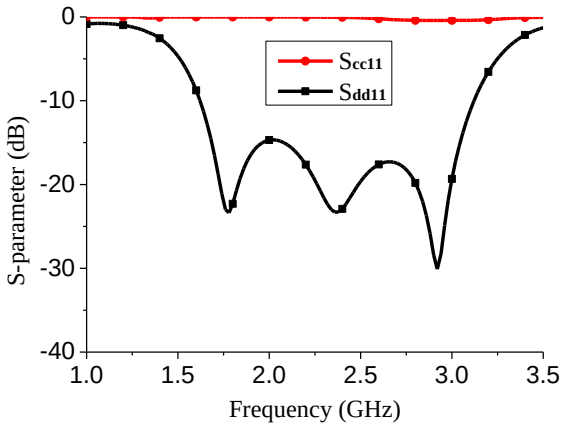

Fig. 10. Simulated differentially driven and commonly driven S-parameters of the antenna.

source impedance of Z_s, and the current loop is formed because of the equivalent short-circuit at P2. As shown in Fig. 8 (b), the input impedance Z_{in} under odd mode excitation can be expressed as

$$Z_{in,odd} = Z_1 \frac{Z_A + jZ_1 tan\theta_1}{Z_1 + jZ_A tan\theta_1} \tag{10}$$

So the reflection coefficient for P1 can be expressed as

$$\Gamma_{1,odd} = \frac{Z_{in,odd} - Z_s}{Z_{in,odd} + Z_s} \tag{11}$$

As a special case, when $Zs=Z_1=Z_A=50$ ohm,

$$\Gamma_{1,odd} = 0 \tag{12}$$

This means that the transmission line equivalent circuit will be well matched when it is excited by the odd mode signal. This is also verified by the simulated results in Fig. 5.

To further illustrate the good transmission under odd mode excitation and high reflection under even mode excitation, Fig. 9 shows the current distributions on the surface of the six-port power divider under even-odd mode excitations. It should be noted that Z_1 and Z_A are designed as 50 ohm based on the above analysis. The current distributions in the figure are shown with the same scale to illustrate the current magnitude. As shown in the figure, when odd mode is excited at P1, transmission mode is excited and the input power is transmitted to the four output ports with the very strong magnitude. Whereas when the even mode is excited at P1, very weak magnitude are excited on the surface of the six-port power divider. The current magnitude ratio between the odd mode and the even mode excitation can

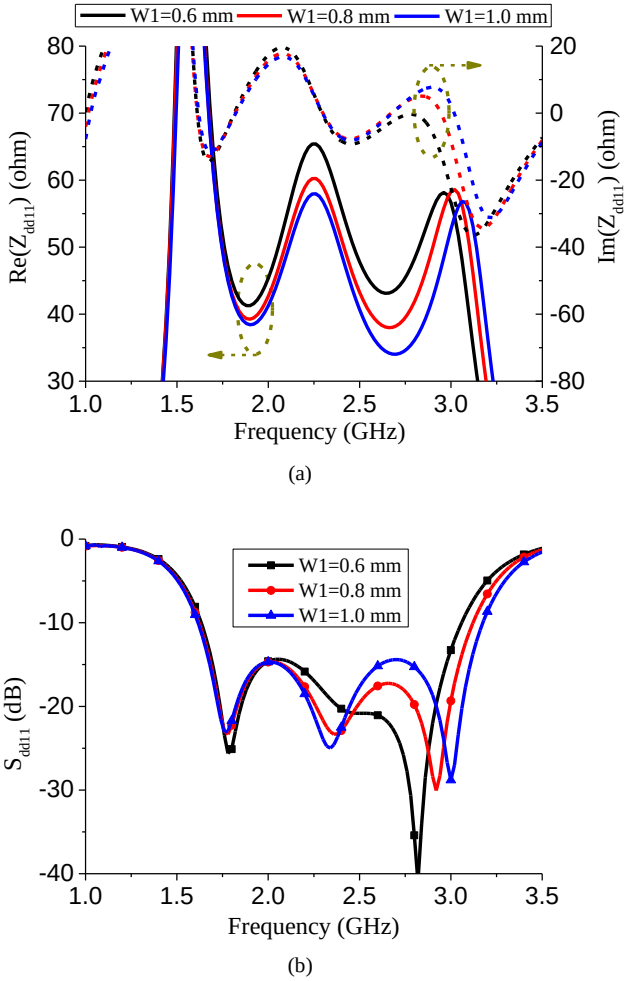

Fig. 11. (a) The input impedance and (b) reflection coefficient of the proposed antenna vary with different W1.

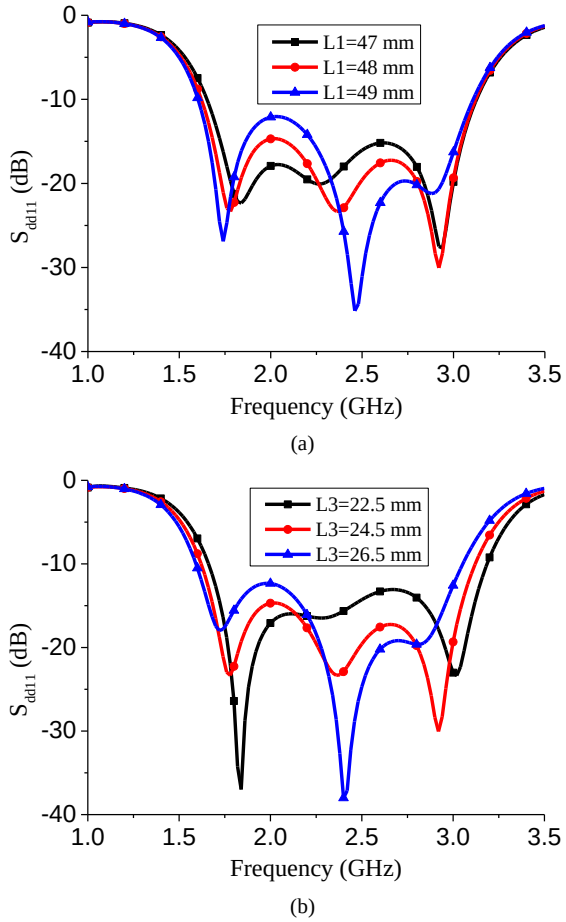

Fig. 12. Simulated S_{dd11} of the proposed antenna varies with different parameters of the proposed antenna. (a) The length of the folded dipole (L1). (b) The distance between the inner edges of the folded dipole (L3).

reach up to almost 200 times. Comparing the two different current distributions, it can be concluded that a good common mode suppression can be obtained by using the proposed six-port power divider.

Combining with the wide impedance bandwidth and the innate even mode suppression of the six-port power divider, wide impedance bandwidth and high common mode suppression can be achieved for the proposed antenna. Fig. 10 shows the simulated differentially driven and commonly driven S-parameters of the antenna. It can be seen that three reflection zeros are achieved on the differentially driven reflection coefficient curve with the wide impedance bandwidth from 1.68 GHz to 3.02 GHz for S_{dd11}<-15 dB. Furthermore, very flat and high suppression is observed over the entire bandwidth with the simulated lowest reflection coefficient higher than -0.42 dB.

E. Antenna Design

The proposed differentially driven dual-polarized antenna is designed based on the above discussed design method. However, it is should be noted that the input impedance of the folded dipole cannot always designed as 50 ohm. Therefore, the offset parallel lines can also function as the impedance transformer. As illustrated by (10), when the electric length of the offset parallel line (θ_1) is equal to 90 degree, the input impedance of the proposed antenna can be expressed as

$$Z_{in} = \frac{Z_1^2}{Z_A} \tag{13}$$

As shown in the configuration of the proposed antenna, when the width of the offset parallel line is changed, its characteristic impedance will be changed as well. The length of the offset parallel line in the design is approximately a quarter of the guided wavelength. Thus, the function of impedance transformer is realized by adjusting the characteristic impedance of the offset parallel lines.

Fig. 11 (a) shows the input impedance of the proposed antenna. As the increase of the width of the offset parallel line, the value of characteristic impedance of Z_1 will be decreased. Therefore, according to (13), the real part of the input impedance of the antenna will also be decreased. The simulated results in this figure agree well with this analysis. Whereas the imaginary part of the input impedance is almost unchanged within the band of interest as the variance of W1. However, it should be noted that the input impedance of the antenna varies noticeably at the higher frequency, compared to the real part at the lower frequency. This is because that the electric length of the transmission line is more sensitive at the higher frequency

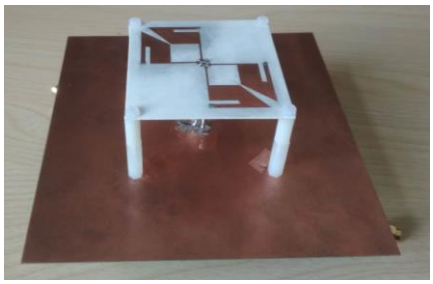

Fig. 13. Photograph of the fabricated prototype of the proposed differentially driven dual-polarized antenna.

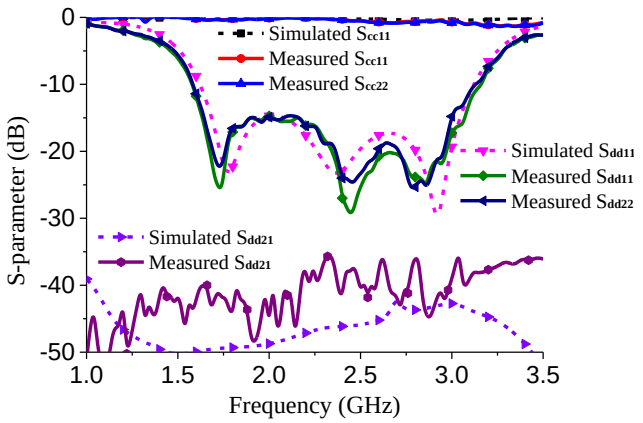

Fig. 14. Measured and simulated S-parameters of the fabricated differentially driven dual-polarized antenna.

region. Therefore, as the increase of W1 shown in Fig. 11 (b), the reflection coefficient at the lower frequency is almost unchanged. Whereas the reflection coefficient at the higher frequency is changed obviously.

In the antenna design process, by changing the length of the folded dipole, the lowest resonant frequency can be changed accordingly. As shown in Fig. 12 (a), as the increase of L1, the first reflection zero shifts to the lower frequency. Under the influence of the increase of L1, the center resonant frequency shifts to the higher frequency. However, the third resonant frequency is almost unaffected. Another should be noted that, the distance between the two inner corners of the folded dipole (L3) is also a key parameter to improve the antenna impedance bandwidth. Fig. 12 (b) shows the simulated refection coefficient varies with different L3. Noted that here L4 is also varied with L3, and the two parameters have the relation of L4=L3-1 mm. It can be seen that, as the increase of the L3, the third reflection zero changes noticeably, which causes the second reflection zero and the third reflection zero moving together. In addition, the first reflection zero moves slightly to the lower frequency as the increase of L3. In brief, by elaborately optimizing these parameters, a wide impedance bandwidth can be achieved for the presented antenna.

III. Results and Discussion

A. Antenna Verification

To validate the above design method, the proposed differentially driven dual-polarized antenna was designed, fabricated, and measured. Fig. 13 shows the photograph of the

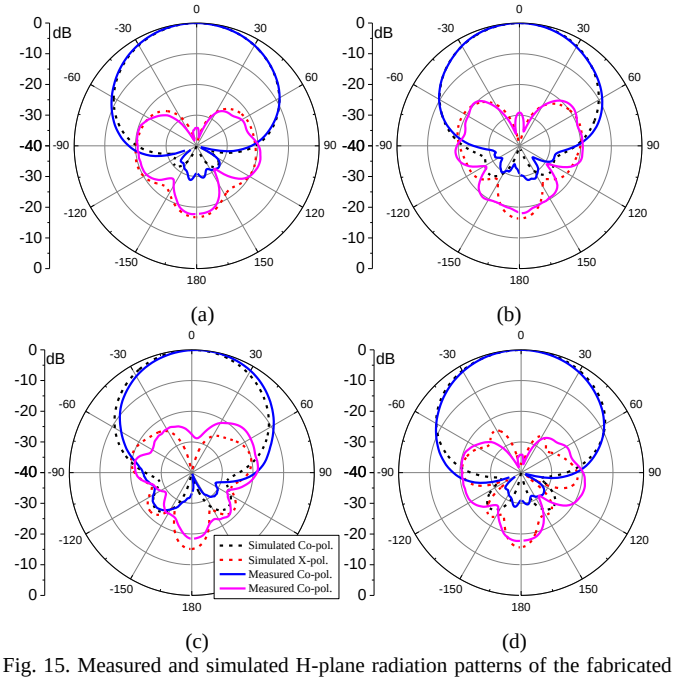

Fig. 15. Measured and simulated H-plane radiation patterns of the fabricated antenna when differentially driven port d1 is excited at different frequencies. (a) 1.7 GHz. (b) 2.2 GHz. (c) 2.7 GHz. (d) 3.0 GHz.

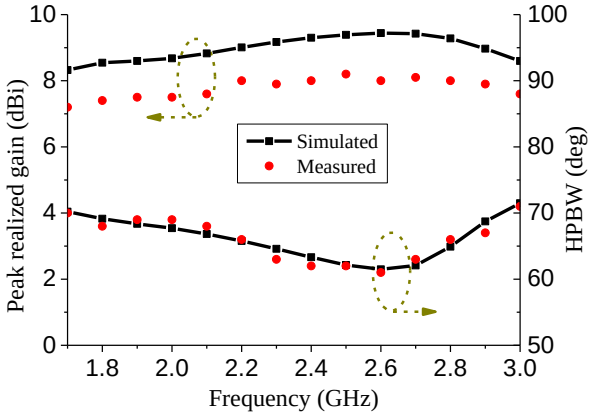

Fig. 16. Measured and simulated peak realized gains and HPBWs of the fabricated antenna.

fabricated prototype. The antenna was measured by using the Anritsu 37397C vector network analyzer and ASYSOL far field antenna measurement system at University of Kent.

Fig. 14 shows the measured and simulated S-parameters of the proposed antenna, including the differentially driven and commonly driven S-parameters. It can be seen that a good accordance can be obtained between the simulated results and the measured results. Owing to the symmetry of the antenna, the simulated S_{dd11} and S_{dd22}, and simulated S_{cc11} and S_{cc22} are almost the same as each other. Therefore, only simulated S_{dd11} and S_{cc11} are given in the figure for comparison. The measured overlapped impedance bandwidth for both S_{dd11} and S_{dd22} lower than -15 dB is from 1.64 to 3.0 GHz. Owing to the symmetrical differentially driven method, the measured isolation is higher than 35.4 dB within the bandwidth. Meanwhile, by using the integrated six-port power divider, very high common mode suppression is achieved with the

TABLE I
COMPARISON OF THE RECENTLY PUBLISHED DIFFERENTIALLY DRIVEN ANTENNAS

Ref.	Overlapped BW (GHz)	RL (dB)	Height (mm)	S_{21} (dB)	CM reflection coefficient (dB)	Pol.
[21]	1.66-2.75 (49.4%)	>15	35	<-37	NG	DP
[22]	1.7-2.75 (48%)	>15	40	<-38	NG	DP
[23]	1.7-2.7 (45.4%)	>14	71.2	<-39	NG	DP
[24]	1.7-2.9 (52%)	>14	34	<-26.3	NG	DP
[25]	1.66-2.8 (51%)	>15	30	<-38	>-1.32	DP
[27]	1.7-2.38 (31%)	>10	35	/	>-1.5	CP
This work	1.64-3.0 (58.6%)	>15	35	<-35.4	>-0.87	DP

BW: Bandwidth. CM: Common Mode. NG: Not Given. DP: Dual-Polarization. CP: Circular Polarization.

measured S_{cc11} and S_{cc22} higher than -0.87 dB over the whole impedance bandwidth.

The measured and simulated normalized radiation patterns are shown in Fig. 15. Because of the symmetry of the antenna, only H-plane radiation patterns excited by differential port d1 are given in the figure. Good agreement can be observed between the simulated and measured radiation patterns. The measured cross-polarization level is 27 dB lower than co-polarized radiation patterns in the broadside direction, and 20 dB lower than the co-polarization radiation patterns within ±30º beamwidth. The measured front to back ratio is higher than 17 dB within the bandwidth. Fig. 16 shows the measured and simulated peak realized gain and half power beamwidth (HPBW) of the antenna. Stable antenna gain and HPBW are achieved within the bandwidth. The measured peak realized gain varies from 7.2 to 8.2 dBi, and the measured half power beamwidth is 66±5º form 1.7 GHz to 3.0 GHz.

B. Comparison

By using the integrated high common mode suppressed six-port power divider, wide impedance bandwidth and high common mode suppression are achieved for the presented differentially driven antenna. Table I compares the recently published differentially driven antennas with the presented antenna. Antennas in [21]-[25] are the differentially driven dual-polarized antennas for base station applications. Owing to the symmetrical differentially driven method, normally high isolation (>35 dB) can be achieved. However, few differentially driven antennas are concerned about the common mode suppression. Whereas the common mode signals would introduce serious noise interference to the circuit systems, and deteriorate the signal-to-noise ratio of the circuit systems. With the help of the additional introduced crossed baluns, high common mode suppression is achieved for the antenna in [25]. However, this can introduce undesired insertion loss and increase the antenna design complexity and fabrication cost. Antenna in [27] is a differentially driven circularly polarized antenna, and the antenna was measured with high common mode suppression. However, its working principle is not clearly illustrated. Compared to these two antennas, the presented antenna keeps simple configuration, but still has much higher suppression and wider impedance bandwidth.

IV. CONCLUSION

This paper proposed a novel method of designing a wideband differentially driven dual-polarized antenna with high common mode suppression. The presented antenna can be equivalent as the combination of a six-port power divider and four crossed folded dipoles. Detailed analysis illustrates that the six-port power divider not only has wide impedance bandwidth under odd mode excitation, but also has high common mode suppression under even mode excitation. Therefore, wide impedance bandwidth and high common mode suppression can be realized for the presented antenna. The measured results demonstrate that a wide impedance bandwidth and high isolation are achieved. Most importantly, high common mode suppression with the common mode reflection coefficient higher than -0.87 dB is also obtained. Both the simulated and measured results prove that the proposed antenna can be a good candidate for the differentially driven base station applications.

REFERENCES

[1] S.-C. Gao, L.-W. Li, M.-S. Leong, and T.-S. Yeo, "Dual-polarized slot coupled planar antenna with side bandwidth," *IEEE Trans. Antennas Propag.*, vol. 51, no. 3, pp. 441–448, Mar. 2003.
[2] L. Wen et al., "A wideband dual-polarized antenna using shorted dipoles," *IEEE Access*, vol. 6, pp. 39725-39733, 2018.
[3] H. Lai and K. Luk, "Dual polarized patch antenna fed by meandering probes," *IEEE Trans. Antennas Propag.*, vol. 55, no. 9, pp. 2625-2627, Sept. 2007.
[4] Y. Gou, S. Yang, Q. Zhu and Z. Nie, "A compact dual-polarized double e-shaped patch antenna with high isolation," *IEEE Trans. Antennas Propag.*, vol. 61, no. 8, pp. 4349-4353, Aug. 2013.
[5] J. Lee, K. Lee and P. Song, "The design of a dual-polarized small base station antenna with high isolation having a metallic cube," *IEEE Trans. Antennas Propag.*, vol. 63, no. 2, pp. 791-795, Feb. 2015.
[6] Y. Guo, K. Khoo and L. C. Ong, "Wideband dual-polarized patch antenna with broadband baluns," *IEEE Trans. Antennas Propag.*, vol. 55, no. 1, pp. 78-83, Jan. 2007.
[7] Hang Wong, Ka-Leung Lau and Kwai-Man Luk, "Design of dual-polarized L-probe patch antenna arrays with high isolation," *IEEE Trans. Antennas Propag.*, vol. 52, no. 1, pp. 45-52, Jan. 2004.
[8] S. Gao and A. Sambell, "Low-cost dual-polarized printed array with broad bandwidth," *IEEE Trans. Antennas Propag.*, vol. 52, no. 12, pp. 3394-3397, Dec. 2004.
[9] H. Li, L. Kang, F. Wei, Y. Cai and Y. Yin, "A low-profile dual-polarized microstrip antenna array for dual-mode OAM applications," *IEEE Antennas Wireless Propag. Lett.*, vol. 16, pp. 3022-3025, 2017.
[10] Y. Wang and Z. Du, "Dual-polarized slot-coupled microstrip antenna array with stable active element pattern," *IEEE Trans. Antennas Propag.*, vol. 63, no. 9, pp. 4239-4244, Sept. 2015.
[11] S. K. Padhi, N. C. Karmakar, C. L. Law and S. Aditya, "A dual polarized aperture coupled circular patch antenna using a C-shaped coupling slot," *IEEE Trans. Antennas Propag.*, vol. 51, no. 12, pp. 3295-3298, Dec. 2003.
[12] S. Gao, L. W. Li, M. S. Leong and T. S. Yeo, "A broad-band dual-polarized microstrip patch antenna with aperture coupling," *IEEE Trans. Antennas Propag.*, vol. 51, no. 4, pp. 898-900, April 2003.
[13] C. Sim, C. Chang and J. Row, "Dual-feed dual-polarized patch antenna with low cross polarization and high isolation," *IEEE Trans. Antennas Propag.*, vol. 57, no. 10, pp. 3321-3324, Oct. 2009.
[14] Kin-Lu Wong and Tzung-Wern Chiou, "Broadband dual-polarized patch antennas fed by capacitively coupled feed and slot-coupled feed," *IEEE Trans. Antennas Propag.*, vol. 50, no. 3, pp. 346-351, March 2002.
[15] Y. Cui, R. Li and H. Fu, "A broadband dual-polarized planar antenna for 2g/3g/LTE base stations," *IEEE Trans. Antennas Propag.*, vol. 62, no. 9, pp. 4836-4840, Sept. 2014.
[16] L. Wen *et al*., "Compact dual-polarized shared-dipole antennas for base station applications," *IEEE Trans. Antennas Propag.* vol. 66, no. 12, pp. 6826-6834, Dec. 2018.

[17] Y. Cui, L. Wu and R. Li, "Bandwidth enhancement of a broadband dual-polarized antenna for 2g/3g/4g and IMT base stations," *IEEE Trans. Antennas Propag.*, vol. 66, no. 12, pp. 7368-7373, Dec. 2018.
[18] Y. Gou, S. Yang, J. Li and Z. Nie, "A compact dual-polarized printed dipole antenna with high isolation for wideband base station applications," *IEEE Trans. Antennas Propag.*, vol. 62, no. 8, pp. 4392-4395, Aug. 2014.
[19] H. Zhai, L. Xi, Y. Zang and L. Li, "A low-profile dual-polarized high-isolation mimo antenna arrays for wideband base-station applications," *IEEE Trans. Antennas Propag.*, vol. 66, no. 1, pp. 191-202, Jan. 2018.
[20] Y. Luo, Q. Chu and D. Wen, "A plus/minus 45 degree dual-polarized base-station antenna with enhanced cross-polarization discrimination via addition of four parasitic elements placed in a square contour," *IEEE Trans. Antennas Propag.*, vol. 64, no. 4, pp. 1514-1519, April 2016.
[21] Z. Tang, J. Liu, Y. Cai, J. Wang and Y. Yin, "A wideband differentially fed dual-polarized stacked patch antenna with tuned slot excitations," *IEEE Trans. Antennas Propag.*, vol. 66, no. 4, pp. 2055-2060, April 2018.
[22] Y. Cui, X. Gao and R. Li, "A broadband differentially fed dual-polarized planar antenna," *IEEE Trans. Antennas Propag.*, vol. 65, no. 6, pp. 3231-3234, June 2017.
[23] Y. Luo and Q. Chu, "Oriental crown-shaped differentially fed dual-polarized multidipole antenna," *IEEE Trans. Antennas Propag.*, vol. 63, no. 11, pp. 4678-4685, Nov. 2015.
[24] D. Wen, D. Zheng and Q. Chu, "A wideband differentially fed dual-polarized antenna with stable radiation pattern for base stations," *IEEE Trans. Antennas Propag.*, vol. 65, no. 5, pp. 2248-2255, May 2017.
[25] Z. Tang, J. Liu, R. Lian, Y. Li and Y. Yin, "Wideband differentially fed dual-polarized planar antenna and its array with high common-mode suppression," *IEEE Trans. Antennas Propag.*, vol. 67, no. 1, pp. 131-139, Jan. 2019.
[26] W. R. Eisenstadt, B. Stengel, and B. M. Thompson, *Microwave Differential Circuit Design Using Mixed-Mode S-Parameters*. Norwood, MA, USA: Artech House, 2006.
[27] Z. Tu, K. Jia and Y. Liu, "A differentially fed wideband circularly polarized antenna," *IEEE Antennas Wireless Propag. Lett.*, vol. 17, no. 5, pp. 861-864, May 2018.

Le-Hu Wen received the M.S. degree in Xidian University, Xi'an, China, in 2011. He is currently working toward the Ph.D. degree with the University of Kent, Canterbury, U.K. His current research interests include multi-band base station antenna, mobile terminal antenna, and tightly coupled array.

Steven Gao (M'01–SM'16-F'19) received the Ph.D. degree in microwave engineering from Shanghai University, Shanghai, China, in 1999.

He is currently a Full Professor and Chair in RF and Microwave Engineering, and the Director of Graduate Studies at the School of Engineering and Digital Arts, University of Kent, UK. His current research interests include smart antennas, phased arrays, MIMO, satellite antennas, satellite communications, UWB radars, synthetic aperture radars, and mobile communications. He is currently an Associate Editor of the IEEE TRANSACTIONS ON ANTENNAS AND PROPAGATION.

Qi Luo (S'08–M'12) is currently a Research Fellow with the School of Engineering and Digital Arts, University of Kent, Canterbury, U.K.

Qingling Yang is currently working toward the Ph.D. degree with the School of Engineering and Digital Arts, University of Kent, Canterbury, U.K.

Wei Hu (S'09–M'14) is currently an Associate Professor with the National Key Laboratory of Antennas and Microwave Technology, Xidian University, Xi'an, China.

Yingzeng Yin (M'16) is currently a Professor with the National Key Laboratory of Antennas and Microwave Technology, Xidian University, Xi'an, China.

Xiaofei Ren is currently a Senior Engineer with the the Innovation and Research Center, China Research Institute of Radiowave Propagation, Qingdao, China.

Jian Wu is currently the Director of the China Research Institute of Radiowave Propagation with the the Innovation and Research Center, China Research Institute of Radiowave Propagation, Qingdao, China.